AIP | Review of Scientific Instruments

A laser system for the parametric amplification of electromagnetic fields in a microwave cavity

A. Agnesi, C. Braggio, G. Carugno, F. Della Valle, G. Galeazzi et al.

Citation: Rev. Sci. Instrum. **82**, 115107 (2011); doi: 10.1063/1.3659950
View online: http://dx.doi.org/10.1063/1.3659950
View Table of Contents: http://rsi.aip.org/resource/1/RSINAK/v82/i11
Published by the American Institute of Physics.

A laser system for the parametric amplification of electromagnetic fields in a microwave cavity

A. Agnesi,[1] C. Braggio,[2,3,a)] G. Carugno,[3] F. Della Valle,[4] G. Galeazzi,[5] G. Messineo,[4] F. Pirzio,[1] G. Reali,[1] and G. Ruoso[5]
[1]*INFN, Sez. di Pavia, Via U. Bassi 6, and Dip. di Elettronica, Univ. di Pavia, Via Ferrata 1, I-27100 Pavia, Italy*
[2]*Dip. di Fisica, Univ. di Padova, Via F. Marzolo 8, I-35131 Padova, Italy*
[3]*INFN, Sez. di Padova, via F. Marzolo 8, I-35131 Padova, Italy*
[4]*INFN, Sez. di Trieste and Dip. di Fisica, Univ. di Trieste, Via A. Valerio 2, I-34127 Trieste, Italy*
[5]*INFN, Lab. Naz. di Legnaro, Viale dell'Università 2, I-35020 Legnaro, Italy*

(Received 22 July 2011; accepted 27 September 2011; published online 22 November 2011)

We describe recent improvements in the development of the high power laser system used in the motion induced radiation (MIR) experiment to amplify electromagnetic fields inside a microwave cavity. The improvements made on the oscillator stabilization, the pulse train shaping device, and the spatial beam uniformity are reported. © *2011 American Institute of Physics*. [doi:10.1063/1.3659950]

I. INTRODUCTION

The aim of the motion induced radiation (MIR) experiment (Ref. 1) is the detection of a quantum effect called the *dynamical Casimir effect*.[2–7] When time dependent boundary conditions are imposed on the electromagnetic fields, generation of real photons is predicted due to amplification of the vacuum fluctuations. This effect should, for example, show up when a mirror moves with a nonuniform acceleration. The energy spectrum of the generated photons is determined by the Fourier components of the mirror motion, the number of photons in each frequency band being larger at higher frequencies. Unfortunately, for any physical mirror, the effect is well below detectability.

It has been shown, however, that the number of photons generated through the dynamical Casimir effect can be enhanced inside a resonator if a parametric resonance condition is fulfilled, namely, for example, when one of the cavity walls oscillates at a frequency $2\nu_0$, where ν_0 is the resonance frequency of the cavity.[8] In the MIR experiment the effect is studied with a high-Q cavity. Since high-frequency mechanical motion of massive cavity walls is a difficult task, the experiment is based on the effective motion[9–11] of a mirror consisting in a semiconductor slab set over one of the walls of the cavity. The reflectivity of the semiconductor is modulated by illuminating it with a train of laser pulses with a repetition rate $f_r \approx 2\,\nu_0$.

The laser repetition frequency f_r fixes the dimensions of the cavity and thus the semiconductor surface that has to be illuminated. A compromise between cavity geometry and laser characteristics is realized with a repetition frequency of the laser pulses in the GHz range. In our set-up the laser working frequency is 4.6 GHz. We are using a superconducting niobium microwave cavity with a cylindrical reentrant geometry, having $\nu_0 = 2.3$ GHz. The semiconductor to be illuminated, a 150 μm-thick disk of GaAs, is placed on top of the reentrant stub, and has a surface of 0.5 cm^2. The material is heavily ion-irradiated to cut the free carriers recombination time down to few picoseconds.[12] The minimum energy per pulse needed to obtain the requested change of the semiconductor mirror conductivity is of the order of a few microjoule.[13,14] Since the average power of a CW laser with this energy per pulse would be too high, we developed a laser delivering a finite train of up to $n \approx 2000$ pulses forming a macropulse with a maximum total duration of $\Delta T = n/f_r \approx 400$ ns.

The laser system should allow to tune the repetition frequency f_r to match the parametric resonance condition: the exact frequency needed is actually shifted from $2\nu_0$ by an amount (∼1 MHz) that has to be experimentally determined.[15] It is then necessary to scan the laser modulation frequency in an interval of a few megahertz centered around $2\nu_0$. The frequency f_r is tuned changing the length of the laser cavity by means of a piezoelectric transducer, as described in Sec. III A. In this operation, the fluctuations of the quantity $\Delta = f_r/2 - \nu_0$ must be kept within the cavity bandwidth, which can be as small as 1 kHz. The microwave cavity is placed inside a liquid Helium cryostat, and its configuration provides a temperature stability that guarantees that the cavity resonance frequency can be regarded as a reference. The *short-term stability* of Δ is then obtained by locking the laser oscillator to an external stabilized microwave generator; this is also described in Sec. III A.

The *long term stability* of the whole laser system is necessary to allow long acquisition periods, as the searched effect is tiny and requires averaging over several measurements performed under the same experimental conditions. This requires that the output macropulse energy should be constant for a few consecutive hours, once it has been set to a value in the interval 10–40 mJ.

A few other parameters of the laser system need to be controlled. All the pulses inside the macropulse must have equal amplitude: a shaping system has been realized and is described in Sec. III B. Moreover, the final laser wavelength should be tunable in the interval 780–820 nm; this feature is necessary to check the dependence of the photon production effect on the excited carriers concentration and/or the thickness of the effective semiconductor mirror.[16]

Few other critical issues are discussed in this paper. In Sec. III C we deal with beam transport from the laser output

a)Electronic mail: caterina.braggio@pd.infn.it.

to the microwave cavity, which requires a correct spatial output beam profile. The problem of uniformly illuminating the semiconductor is finally discussed in Sec. IV.

II. LASER SYSTEM

The laser system, schematically shown in Fig. 1, is based on a master oscillator-power amplifier architecture. The master oscillator generates the seed signal and the optical amplifier chain boosts it to the required output power.[17]

The master oscillator (M-OSC box in Fig. 1) is a V-folded cavity of about 3 cm length, delivering pulses of 6 ps duration at a rate of about 4.6 GHz. The oscillator is CW passively mode-locked by means of a saturable absorbing mirror (SAM), acting also as end cavity mirror. The output wavelength is 1064 nm. For further details, the reader should refer to our paper,[18] where a prototype of this oscillator, working at lower frequency, is described.

From the continuous train emitted by the master oscillator a finite number of pulses (macropulse) is selected by means of an acousto-optic modulator (AOM). The selected pulses are then amplified in a two-step optical amplifier. The pre-amplifier stage comprises two Nd:YVO_4, 1% doped slabs, each side-pumped by a pulsed 150-W peak power laser diode array in a grazing incidence, total internal reflection configuration. The single-pass, small-signal gain in this stage is higher than 60 dB, with a well preserved beam quality ($M^2 = 1.2$); pulse duration is slightly increased to 8.9 ps. For the second amplification stage, two 12-cm long, 6-mm diameter, flash-lamp pumped, 1% doped Nd:YAG rods are employed, with a net small-signal gain of 33 dB; after this stage the pulses have a duration of 12 ps.

To excite carriers at the bottom of the conduction band in GaAs, a wavelength of approximately 800 nm is requested.[16] For this reason, after the power amplifier chain, the 1064 nm beam undergoes second harmonic generation in a lithium triborate (LBO) crystal and is then used to synchronously pump a plane-plane cavity optical parametric oscillator (OPO), in which both the OPO mirrors and the crystal coatings are designed to obtain a singly resonant oscillator operating around 800 nm. By interchanging two differently cut potassium titanyl phosphate (KTP) crystals, two ranges of wavelengths (780–800 nm and 800–820 nm) can be spanned. A scheme

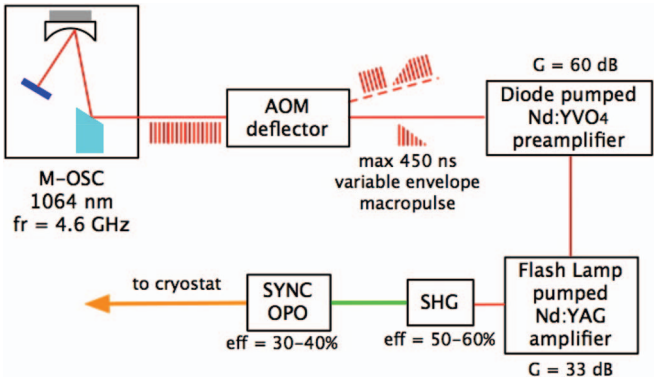

FIG. 1. (Color online) Conceptual setup of the laser system.

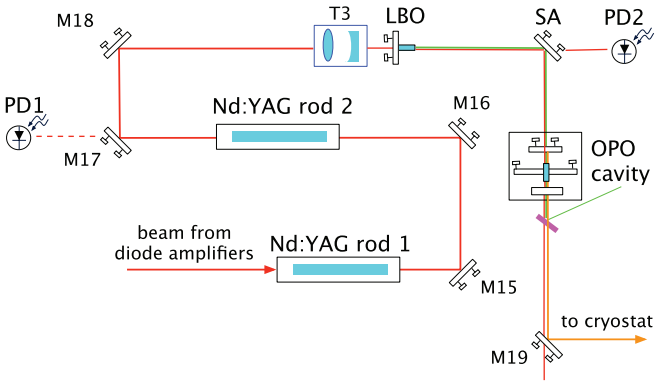

FIG. 2. (Color online) Scheme of the Nd:YAG rod amplifier and wavelength conversion sections of the laser. After amplification at constant section in the rods, the beam is reduced in size by the telescope T3 (magnification $M = 0.5$) to increase the conversion efficiency in a LBO crystal (dimensions: $4 \times 4 \times 15$ mm^3). An harmonic separator (SA) reflects the 532 nm light to pump an OPO cavity. The mirror M19 transmits the idler beam and reflects the signal wavelength to the cryostat outside the clean room. Photodiodes PD1 and PD2 monitor the macropulse shape, respectively, before and after second harmonic generation.

of the Nd:YAG rod amplifier and wavelength conversion sections of the laser is shown in Fig. 2. The output pulse width is 7.2 ps (see Fig. 3).

The laser system operates in a clean, temperature-controlled room. It is mounted on an optical table with active air-spring vibration isolation supports to minimize seismic vibrations. The master oscillator components are mounted on a massive Al block to improve its mechanical and thermal stability. Besides, in the clean room, temperature changes are kept within 1 K per day. The output beam is directed through an optical window to an adjacent room where the experiment cryostat is set-up.

III. LASER OPTIMIZATION

A. Stabilization of the master oscillator

The repetition rate f_r of the laser is determined by the master oscillator length L through the relation $f_r = c/2L$, with

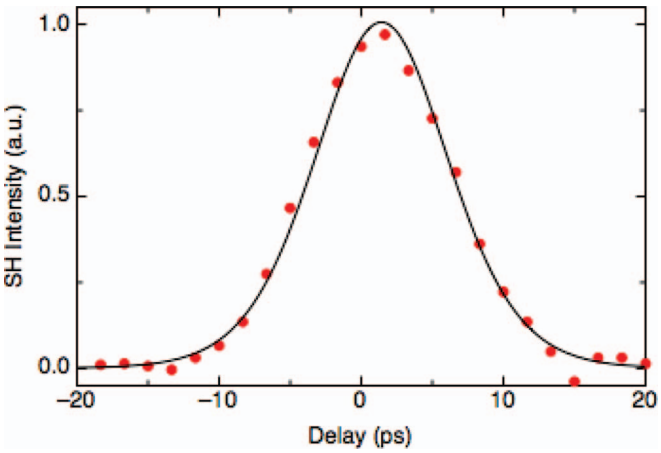

FIG. 3. (Color online) (Dots) Autocorrelation measurement of the laser pulse width after the OPO stage. The continuous line is the best fit obtained with a squared hyperbolic secant function, corresponding to a pulse width of 7.2 ps.

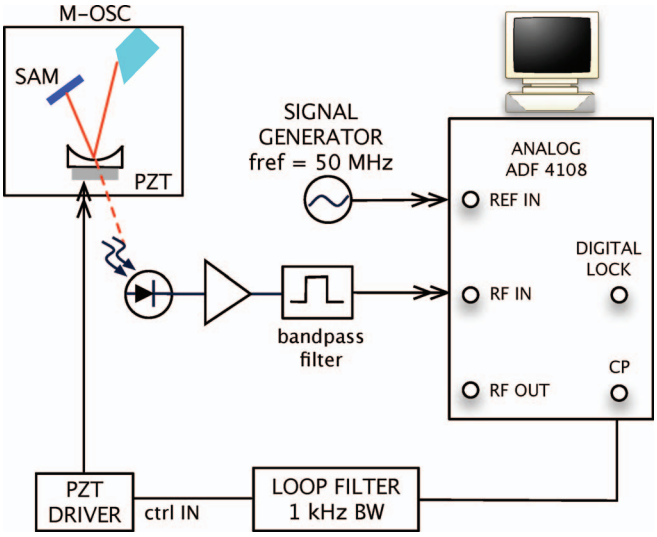

FIG. 4. (Color online) Scheme of the electronic feedback used to stabilize the master oscillator repetition frequency. A fast photodiode monitors the oscillator output, which is compared to a reference microwave generator inside the frequency synthesizer ADF4108. Its output controls the high voltage fed to a piezoelectric transducer (PZT) which adjusts the length of the cavity.

c the light speed. In our 3 cm long cavity we have seen that mechanical perturbations can produce a jitter up to a few hundreds hertz. Moreover, drifts of thermal origin can also influence the cavity geometry to such an extent that the oscillator exceeds the stability band for the mode-locking operation. To ensure the required long and short term stability, the master oscillator length is actively controlled by the feedback system shown in Fig. 4.

The repetition rate of the laser is locked to an external microwave generator by means of a digital phase-locked loop. The laser repetition rate and the reference signal are compared in a phase-frequency detector, generating an error signal to be fed to a piezoelectric crystal (PZT) which adjusts the length of the cavity. The PZT is mounted on the back of the folding mirror of the cavity; by changing the dc signal fed to the piezo it is thus also possible to choose the repetition frequency, as shown in Fig. 5.

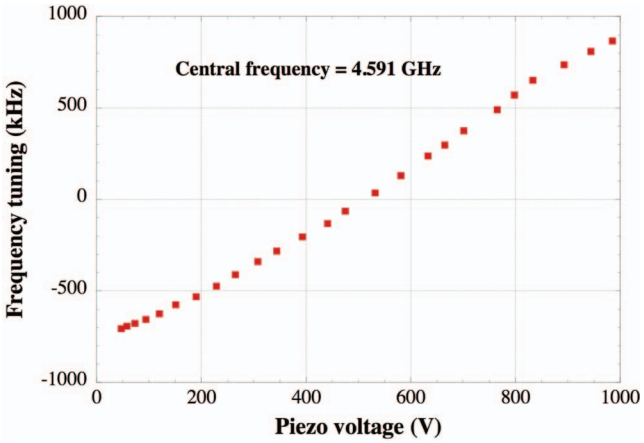

FIG. 5. (Color online) Tuning of the repetition rate around the central frequency. The maximum change that can be obtained is 1.6 MHz.

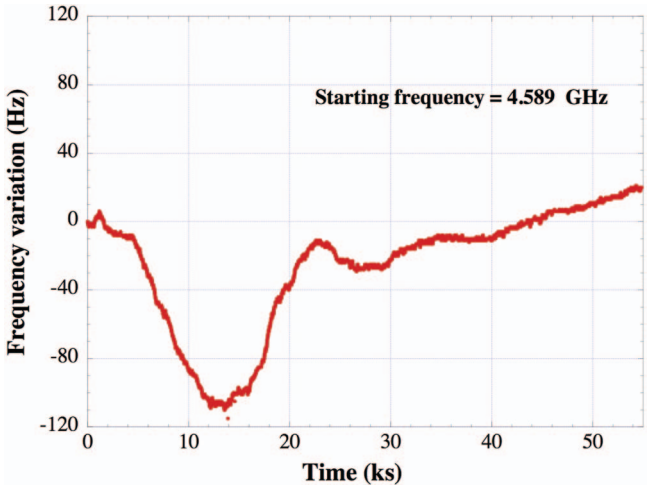

FIG. 6. (Color online) A 15-h measurement of the master oscillator frequency stability obtained with an Agilent spectrum analyzer ESA E 4405-B.

The feedback is based on the Analog Devices ADF4108 frequency synthesizer. The oscillator repetition frequency is obtained by means of a fast photodiode, which monitors one of the two 1% optical losses of the folding mirror; this signal is then amplified to a level of −10 dBm and fed to the ADF4108 input, after the passage through a bandpass filter to reduce the noise. The ADF4108 digitally divides the frequency of the reference signal by a factor R, and the one of the laser signal by a factor N, and then compares frequency and phase of the divided signals.[19] This digital phase frequency detection (PFD) produces an error output current which depends on this comparison: if the phase difference between the two signals is small, the PFD circuit generates a proportional current; if the two frequencies are far away from each other, the output saturates and tells the sign of the frequency difference. The error current is filtered and converted to a voltage signal for the PZT.

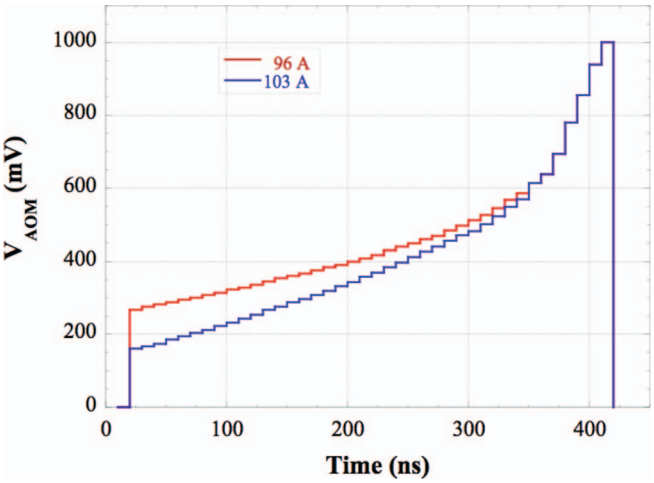

FIG. 7. (Color online) Plot of the AOM driver function, for two different values of current delivered to the diodes in the pre-amplifier stage. The function is stepwise with a 10 ns discretization time. The lower curve, corresponding to 103 A, allows to extract a greater macropulse energy.

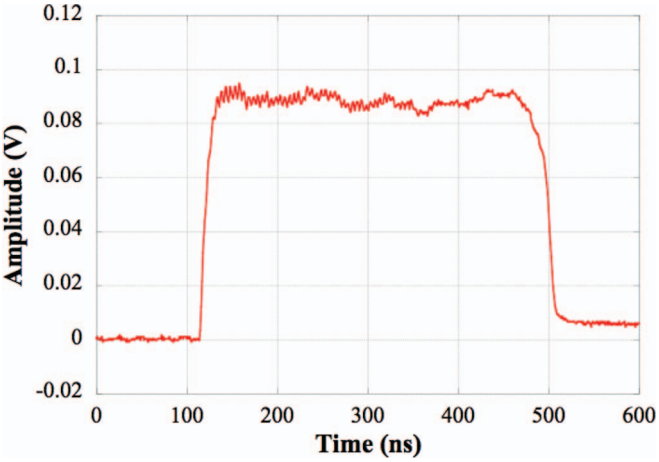

FIG. 8. (Color online) Oscilloscope trace of the train of laser pulses emerging from the OPO cavity at about 800 nm, taken with a 50 ps rise time photodiode (Hamamatsu C4258) placed after the engineered diffuser (see Sec. IV). The horizontal scale is 50 ns/division. The limited sampling of the oscilloscope does not allow to reproduce accurately each single 12 ps pulse.

In Fig. 6, we show a 15 h long measurement of the repetition frequency: the frequency drifts less than 150 Hz during the entire time span.

B. Pulse train envelope control

A finite number of pulses from the oscillator output is selected by the AOM to form the macropulse, as pictorially shown in Fig. 1. If a flat-top macropulse is injected into the amplifier chain, envelope shape distortions develop in the output macropulse due to amplifier saturation effects.[20] In order to obtain an homogeneous output from the amplifiers, the pulses in the leading edge of the input macropulse have to be smaller than those in the trailing edge, as the latter encounter a smaller inverted population in the amplifier. This can be done by shaping the AOM driving voltage as shown in Fig. 7. This curve is obtained by using an iterative procedure. An arbitrary function generator is programmed and the waveform is modified until the photodiode PD1 in Fig. 2 measures a flat output macropulse after the Nd:YAG rod amplification stage. Different compensating functions are needed for each value of the current of the diode amplifiers. Note also that the amplification of the Nd:YAG rods strongly depends on the beam area and the path, which both can slightly change after realignments of the master oscillator, thus requiring an adjustment of the macropulse shaping function on a few days basis.

Figure 8 shows the train emerging from the OPO cavity at approximately 800 nm taken with a 50 ps rise time photodiode and recorded at a 6 GHz bandwidth oscilloscope. The energy of the pulses belonging to a macropulse is uniform within 10%: there is a significant improvement of the train of pulses uniformity compared to the previous electronic scheme.[17]

C. The beam profile

After wavelength conversion, the laser beam has to travel a distance ≈4 m to reach the cryostat in which the MIR experimental apparatus is enclosed. The beam then enters the microwave cavity through a 1.8 mm diameter opening, to shine onto a semiconductor disk of 8.4 mm diameter. A properly shaped output beam profile is then necessary in order to have a correct propagation along the optical path.

The beam quality is preserved until the end of the first stage of amplification,[17] but can be lost in the subsequent sections, due to phenomena taking place in the second amplification stage (Nd:YAG rods) and in the OPO cavity.

In order to obtain maximum amplification from the Nd:YAG rod amplifiers, the usual condition to be met is $3\omega_0 \gtrsim \phi$, where ω_0 is the beam waist and ϕ the rod diameter. However, with such a choice, the laser rods aperturing the beam introduce diffraction rings. These rings are strong intensity modulations which are not only undesirable for the beam propagation, but can also cause optical damage in the following elements, in particular in the nonlinear crystals which are used to make wavelength conversion.

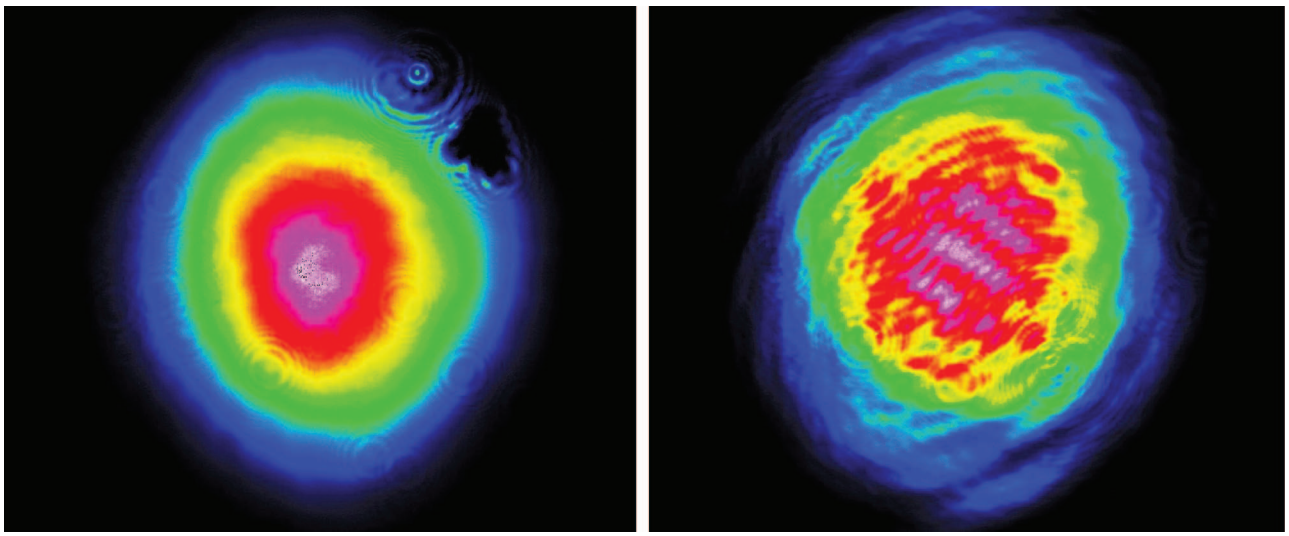

FIG. 9. (Color online) Laser beam profile: (left) before entering the Nd:YAG rods; (right) after passing through the two rods; diffraction patters are kept within acceptable limits.

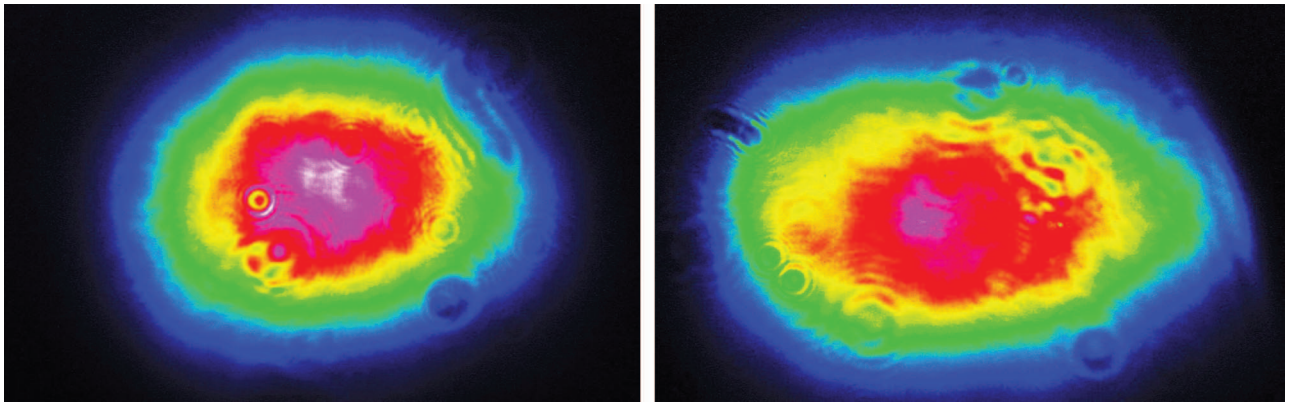

FIG. 10. (Color online) Optical parametric oscillator output for two different pump energies: (left) 20 mJ macro-pulse total energy; (right) 40 mJ macro-pulse total energy.

In our laser system we have chosen instead to have $3\omega_0 < \phi$. This provides an infrared train of pulses with total energy still greater than 200 mJ, large enough for our needs, and characterized by not too marked modulation patterns. In Fig. 9, a laser beam profiler analysis of the beam before and after the two Nd:YAG rods is shown.

The optical parametric oscillator cavity is a second critical element of spatial beam deterioration. In fact, once the OPO cavity has been aligned for oscillation, we have observed that in correspondence of larger values of the energy in the pump beam, the divergence of the beam increases in the plane of the phase matching of the KTP crystal. The resulting profile is markedly elliptical for a macro-pulse output energy of approximately 40 mJ (see Fig. 10), this effect being less evident for 20 mJ. An increasing divergence of the beam in the plane of the phase matching for greater pump beam intensities has been found also by other authors in similar configurations.[21–23] Being this phenomenon intrinsic to the mechanism of OPO generation in the required energy range (30–40 mJ), a possible solution is the use of a galilean telescope made of cylindrical lenses at the output of the OPO cavity when using large output energies. For the time being we limit the laser energy to values smaller than 20 mJ.

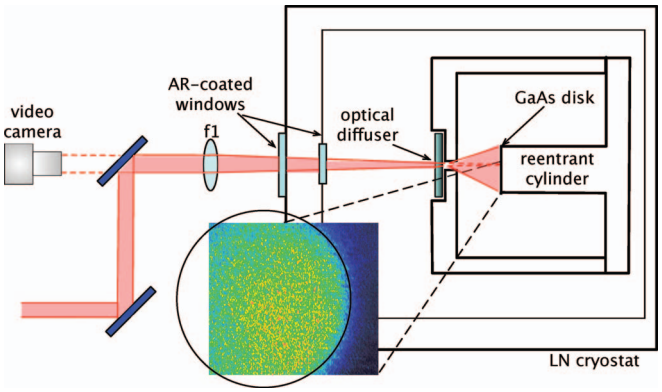

FIG. 11. (Color online) Optical scheme to uniformly illuminate the semiconductor. The laser beam is focused onto the surface of the GaAs disk through an engineered diffuser. The square inset shows the power density at the semiconductor surface, recorded with a CCD camera set at the position of the GaAs disk. The circle defines the area to be illuminated.

IV. SEMICONDUCTOR SLAB ILLUMINATION

The microwave cavity we are using is a cylindrical one with a reentrant stub. The semiconductor to be illuminated is placed on top of the stub, a few millimeters away from the hole through which the laser beam enters into the cavity (see Fig. 11). A uniform concentration of carriers over the semiconductor surface is recommended, since regions characterized by a lower concentration of carriers are subject to a greater electromagnetic field dissipation, critical for the photon amplification process.[14] Since a gaussian beam profile does not provide a uniform illumination pattern, we developed the optical system shown in Fig. 11. The incoming beam is focused at the semiconductor disk position with the lens f1; before focus, at the cavity aperture, the beam passes through an engineered diffuser, namely, a microlenses array with 40° divergence angle. The diffuser shapes the beam to a circular pattern corresponding to the semiconductor disk dimension. The inset in Fig. 11 shows the illumination profile obtained at the GaAs surface position; the area is uniformly illuminated, even at the border of the disk, where dissipation effects inside the semiconductor are even more detrimental since there the electromagnetic field reaches the maximum intensity.

For alignment purposes, the diffuser is apertured with a metallic ring: the light reflected from the ring is monitored with a video camera and the alignment corresponds to a minimum of the reflected intensity.

V. CONCLUSIONS

We have optimized the performances of an amplitude modulated laser system in order to meet critical requests for its use as the primary light source in an experiment searching for the dynamical Casimir effect. Trains of about 2000 pulses (macropulses) can be produced with a tunable repetition rate of about 4.6 GHz, frequency stable within 100 Hz over several hours. The output wavelength is around 800 nm, tunable over a 40 nm range. A single macropulse has energy of several tens of millijoule, uniformly distributed along its time duration. Finally, a properly chosen beam transport and profiling allows for an optimum illumination of a target circular area of 8.4 mm diameter.

ACKNOWLEDGMENTS

This work was in part supported by the Casimir Network of the European Science Foundation. C.B. and G.M. acknowledge support by the Schwinger Foundation.

The authors thank M. Prevedelli for his precious suggestions in the development of the feedback system, and gratefully acknowledge technical support by E. Berto, D. Corti, and F. Zatti.

[1] C. Braggio, G. Bressi, G. Carugno, C. Del Noce, G. Galeazzi, A. Lombardi, A. Palmieri, G. Ruoso, and D. Zanello, Europhys. Lett. **40**, 754 (2005).
[2] G. T. Moore, J. Math. Phys. **11**, 2679 (1970).
[3] S. A. Fulling and P. C. W. Davies, Proc. R. Soc. London, Ser. A **348**, 393 (1976).
[4] G. Barton and C. Eberlein, Ann. Phys. **227**, 222 (1993).
[5] J. Schwinger, Proc. Natl. Acad. Sci. U.S.A. **89**, 4091 (1992).
[6] V. V. Dodonov, Phys. Scr. **82**, 038105 (2010).
[7] D. A. R. Dalvit, P. A. Maia Neto, and F. D. Mazzitelli, "Fluctuations, Dissipation and the Dynamical Casimir Effect," Chap. 13 in *Casimir Physics*, edited by D. Dalvit, P. Milonni, D. Roberts, and F. da Rosa, Lecture Notes in Physics Vol. 834 (Springer Verlag, Berlin, 2011).
[8] A. Lambrecht, M.-T. Jaekel, and S. Reynaud, Phys. Rev. Lett. **77**, 615 (1996).
[9] E. Yablonovitch, Phys. Rev. Lett. **62**, 1742 (1989).
[10] Y. E. Lozovik, V. G. Tsvetus, and E. A. Vinogradov, Phys. Scr. **52**, 184 (1995).
[11] Y. E. Lozovik, V. G. Tsvetus, and E. A. Vinogradov, JETP Lett. **61**, 723 (1995) [Pis'ma Zh. Eksp. Teor. Fiz. **61**, 711 (1995)].
[12] J. Mangeney, N. Stelmakh, F. Aniel, P. Boucaud, and J.-M. Lourtioz, Appl. Phys. Lett. **80**, 4711 (2002).
[13] C. Braggio, G. Bressi, G. Carugno, A. Lombardi, A. Palmieri, G. Ruoso, and D. Zanello, Rev. Sci. Instrum. **75**, 4967 (2004).
[14] C. Braggio, G. Bressi, G. Carugno, A. V. Dodonov, V. V. Dodonov, G. Galeazzi, G. Ruoso, and D. Zanello, Phys. Lett. A **363**, 33 (2007).
[15] V. V. Dodonov, J. Phys.: Conf. Ser. **161**, 012027 (2009).
[16] M. D. Sturge, Phys. Rev. **127**, 768 (1962).
[17] A. Agnesi, C. Braggio, L. Carrà, F. Pirzio, S. Lodo, G. Messineo, D. Scarpa, A. Tomaselli, G. Reali, and C. Vacchi, Opt. Express **16**, 15811 (2008).
[18] A. Agnesi, F. Pirzio, A. Tomaselli, G. Reali, and C. Braggio, Opt. Express **13**, 5302 (2005).
[19] M. Curtin and P. O'Brian, Analog Dial. **33**, 9 (1999).
[20] L. M. Frantz and J. S. Nodvik, J. Appl. Phys. **34**, 2346 (1963).
[21] B. Bourliaguet, A. Mugnier, V. Kermène, A. Barthély, and C. Froehly, Opt. Commun. **167**, 177 (1999).
[22] V. L. Naumov, A. M. Onishchenko1, A. S. Podstavkin, and A. V. Shestako, Quantum Electron. **30**, 632 (2000).
[23] G. Anstett, G. Göritz, D. Kabs, R. Urschel, R. Wallenstein, and A. Borsutzky, Appl. Phys. B **72**, 583 (2001).